8

Planetary Geodynamics

Planetary bodies dynamically respond to applied stresses. Heat transfer out of the interior commonly leads to stresses that affect the surface. For quantitative analysis of geodynamics, numerical techniques are generally required and are applied looking at the material as a continuum. Rocks and ice in planetary bodies ultimately want to be in equilibrium with applied stresses. Equilibrium can be assessed by computing whether the stress gradients balance the applied force. The material response to stress is strain, which can be calculated from displacement gradients throughout the material. Stress and strain in a solid are related through intrinsic material properties (e.g., Young's modulus and Poisson's ratio). The material properties of rock and ice are similar enough that the icy lithospheres of the moons of the outer planets undergo the same basic processes as the rocky lithospheres of the terrestrial planets. Large lithospheric blocks are supported isostatically, floating in the asthenosphere. Topography can also be supported by the strength of the lithosphere, in which case some amount of flexure occurs as a result of the load on the surface. The distribution of mass in the subsurface can be inferred from measurements of the gravity field. From such measurements, it is possible to discern if a feature such as a mountain or volcano has a large root, or if a large mass lies beneath a surface with no topography (e.g., lunar mascons). Surface temperature is controlled for most planetary surfaces by solar heating, the effect of which generally only penetrates a few meters into the surface. Heat flows through the brittle lithosphere by conduction, but the deeper asthenosphere transfers heat through convection. The asthenosphere behaves like a fluid on geologic timescales, and its response to stress must be investigated in terms of fluid mechanics. The exact response to stress, or the rheology, depends on many factors, including temperature, composition, grain size, and the magnitude of stress. The ductile behavior of the

interior is coupled to the surface, enabling geodynamicists to use observations of the surface to infer properties of the interior.

8.1 Motions in Planetary Interiors

Planetary surfaces are, in many ways, shaped by properties of their interiors and motions below their surfaces. Those properties and motions are strongly controlled and driven by planetary heating and heat trying to get out of the interior. Chapter 6 introduced planetary heating, and Chapter 7 introduced planetary interiors. We now want to take a look at techniques that are used to understand the dynamics below the surfaces of planets and the effects on the surfaces that spacecraft, and maybe eventually astronaut geologists, study.

Earth's surface, for example, is very geologically active, and most of that activity is explained in the framework of plate tectonics. Earth's surface plates move relative to each other (at rates of about 5 to 10 cm/yr, in general), and those motions induce a lot of stress in the lithosphere. If we look more deeply, we see that plate motions are driven by convection working to transfer heat from Earth's deep interior to its surface, to ultimately be radiated to space. Examining the rest of the Solar System, though, we do not see any clear evidence of global plate tectonics taking place on any other body. Does that mean that their interiors are cold and inactive? Certainly not.

Dramatic examples such as the pervasive volcanism on Io and the active geysers erupting from the south pole of Enceladus tell us that even small moons can have dynamic interiors. Geologic features such as large rift systems, mountains, and volcanoes on Venus, global thrust faults on Mercury, giant volcanoes and rifts on Mars, relaxed topography and fault systems on icy satellites, and apparently active convection in surface nitrogen ice on Pluto make it clear that intense forces are or have

been acting on surfaces throughout the Solar System. This chapter introduces concepts, and their quantitative foundation, needed to investigate and understand motions in planetary interiors and how those affect planetary surfaces.

8.2 Geologic Stresses and Deformations

Force balance is fundamental to understanding the equilibrium state of a body and for investigating what happens in non-equilibrium conditions. Our goal is to compute deformation within a solid planetary surface for given stresses. Alternatively, we may be interested in the inverse problem – determining from the observed deformation state what stresses must be, or have been, acting within the solid portion of a planetary body. Rocks and ices under relatively small stresses generally display linear **elastic behavior**. Such behavior is the domain of classical elasto-statics (for the equilibrium case) and elasto-dynamics (for non-equilibrium situations). Later on (Section 8.6), we'll look at the case of more fluid-like (**ductile**) behavior. Section 9.2 discusses these behaviors in the context of observed structures and tectonics. Elasto-statics/-dynamics consists of three components (or sets of equations): (1) stress equilibrium (i.e., force balance or momentum conservation), (2) definition of strain in terms of continuum deformations, and (3) constitutive equations that relate stress and strain in a solid. To solve these sets of equations quantitatively, particularly numerically (the common approach of modern geophysics/geodynamics), geodynamicists work in the domain of **continuum mechanics**.

8.2.1 Balancing Act: Stress Equilibrium

Stress (σ) is defined as a force divided by the area over which the force acts. Figure 8.1 shows the stress components on an infinitesimally small volume inside some solid (e.g., a planetary lithosphere). *Normal stresses* are those that act perpendicular to one of the surfaces of the volume (i.e., along the surface normal vector), and *shear stresses* are those that act parallel to the surface. The force
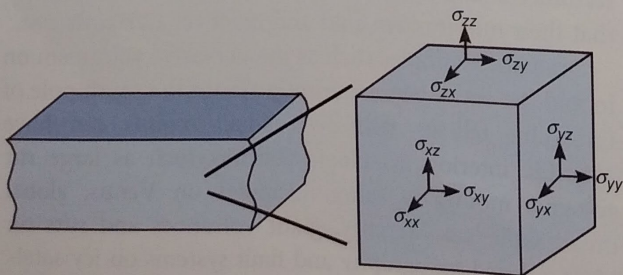
Figure 8.1 Illustration of the normal and shear components of stress acting on an infinitesimally small volume within a planetary surface.

acting on each surface can be decomposed into one normal stress and two shear stresses that are all orthogonal to one another. Customarily, the first subscript refers to the direction of the surface normal, and the second to the direction of the force (but conventions vary in different fields, so it is always necessary to check conventions). Because there are no internal torques, $\sigma_{xy} = \sigma_{yx}$, $\sigma_{xz} = \sigma_{zx}$ and $\sigma_{yz} = \sigma_{zy}$, leaving six independent stress components of three normal stresses and three shear stresses.

Using the infinitesimal volume in Figure 8.1, it is possible to show that for the volume to be in equilibrium, any outside applied force in each dimension must balance the sum of normal and shear **stress gradients** in that dimension. This equilibrium state is expressed mathematically as the following set of equations:

$$f_x = \frac{\partial \sigma_{xx}}{\partial x} + \frac{\partial \sigma_{yx}}{\partial y} + \frac{\partial \sigma_{zx}}{\partial z}$$
$$f_y = \frac{\partial \sigma_{xy}}{\partial x} + \frac{\partial \sigma_{yy}}{\partial y} + \frac{\partial \sigma_{zy}}{\partial z} \qquad (8.1)$$
$$f_z = \frac{\partial \sigma_{xz}}{\partial x} + \frac{\partial \sigma_{yz}}{\partial y} + \frac{\partial \sigma_{zz}}{\partial z}$$

where f_x, f_y, and f_z are the external applied forces per unit volume in each dimension. In the common static case within a planetary surface, the primary external force is gravity. Box 8.1 includes an illustration of how to use the stress equilibrium equations to solve for a continuous expression for stress.

8.2.2 What Exactly Is Strain?

When a stress is applied to an object or mass of material, the material will deform. This deformation is called **strain** (ε). Like stress, strain has normal and shear components. In macroscopic terms, normal strain is generally defined as the change in length of a body in a given dimension to the original length in that dimension, and shear strain as the change in angles between faces of the body.

In continuum mechanics, strain is defined by the relative displacements of points within the body (Figure 8.2). If all points move the same amount, there is no relative displacement, just an overall translation or rotation of the body. The important quantities are, again, gradients – in this case, displacement gradients. Normal strains are defined as

$$\varepsilon_{xx} = \frac{\partial u_x}{\partial x}$$
$$\varepsilon_{yy} = \frac{\partial u_y}{\partial y} \qquad (8.2)$$
$$\varepsilon_{zz} = \frac{\partial u_z}{\partial z}$$

where u_x, u_y, and u_z are the displacements in each dimension. The shear strains are defined as
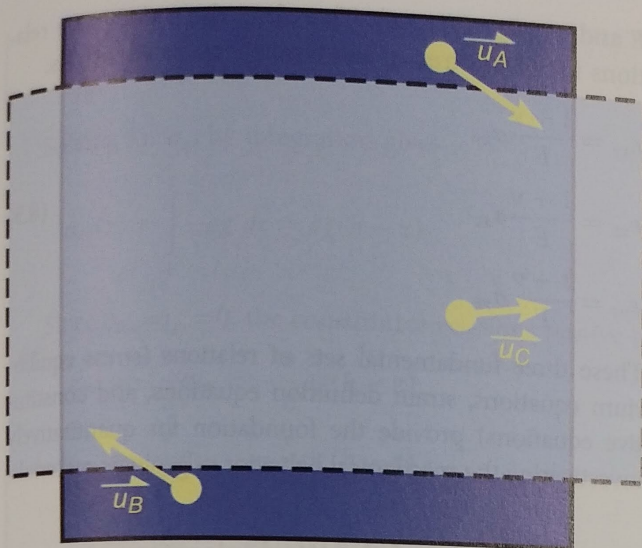
Figure 8.2 Illustration of displacement vectors within a strained volume. Dark blue (solid outline) represents the original shape. In order to deform to the light blue shape (dashed outline), points within the volume must move. Displacement gradients are found by computing differences between the displacement vectors of points within the volume.

$$\varepsilon_{xy} = \frac{1}{2}\left(\frac{\partial u_x}{\partial y} + \frac{\partial u_y}{\partial x}\right)$$

$$\varepsilon_{xz} = \frac{1}{2}\left(\frac{\partial u_x}{\partial z} + \frac{\partial u_z}{\partial x}\right) \tag{8.3}$$

$$\varepsilon_{yz} = \frac{1}{2}\left(\frac{\partial u_y}{\partial z} + \frac{\partial u_z}{\partial y}\right)$$

Similar to the case with stresses, the complementary shear strains are equal to each other (i.e., $\varepsilon_{xy} = \varepsilon_{yx}$, $\varepsilon_{xz} = \varepsilon_{zx}$, and $\varepsilon_{zy} = \varepsilon_{yz}$).

8.2.3 Relating Stress and Strain

Now that we can relate deformation (displacements) to strains and compute stresses from applied forces, we need to be able to relate stress and strain to each other. Solid geologic materials near the surfaces of the Earth and other planetary bodies generally respond elastically to applied stresses (so long as the stresses are not too large). Rock (or ice) will deform when stress is applied, but will return to its original shape when the stress is removed. Furthermore, the response is generally linear – doubling the stress will double the strain. This behavior is sketched schematically in Figure 8.3.

Mathematically, linear elasticity is similar to stretching and compressing a spring, so Hook's law applies. The relation of normal stresses to normal strains in the same dimension can be written as $\sigma_{xx} = E\varepsilon_{xx}$, where the proportionality constant E is called *Young's modulus*. It is a property that describes how stiff a material is with respect to tension or compression. Since strain is a dimensionless quantity, E must have the same units as stress (i.e., force
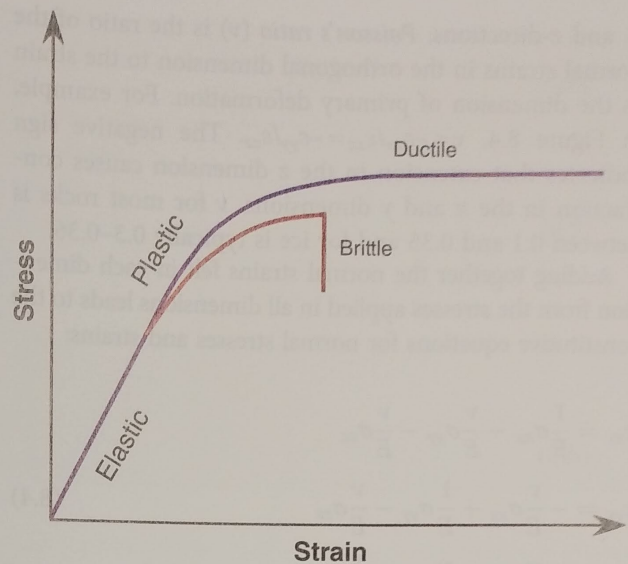
Figure 8.3 Schematic illustration of the relationship between stress and strain in most solid geologic materials. For small stress and strain, the relationship is linear and elastic. Eventually, the amount of strain is such that it cannot be recovered (plastic) and the relationship becomes nonlinear. If the stress overcomes the strength of the material plus confining pressure, fracturing occurs (brittle). Otherwise, the material will flow to accommodate applied stress (ductile).
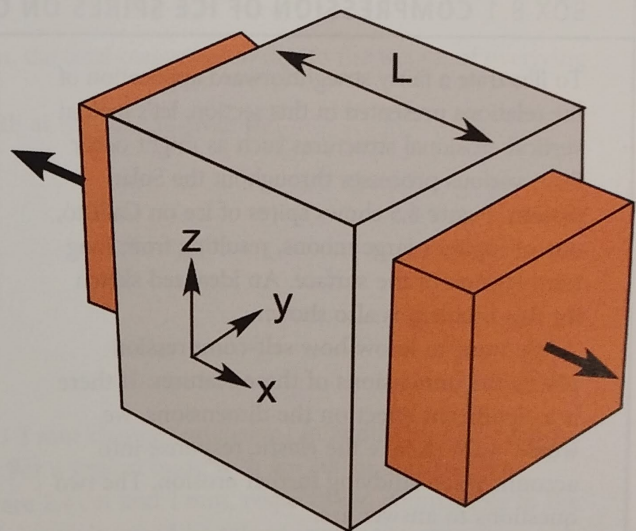
Figure 8.4 Deformation (extension or compression) in one dimension causes deformation in the orthogonal dimensions. This effect is parameterized by Poisson's ratio.

per area, or pressure). E for rocks is typically ~40–80 GPa and for ice is ~6–12 GPa.

In real materials, normal strain in one dimension leads to a normal strain in the orthogonal dimensions. This behavior is illustrated in Figure 8.2, where the original square compresses in the vertical direction and extends in the horizontal, and in Figure 8.4, where the cube extends in the x-direction and correspondingly compresses in the

y- and z-directions. *Poisson's ratio* (v) is the ratio of the normal strains in the orthogonal dimension to the strain in the dimension of primary deformation. For example, in Figure 8.4, $v = -\varepsilon_{xx}/\varepsilon_{zz} = -\varepsilon_{yy}/\varepsilon_{zz}$. The negative sign indicates that extension in the z dimension causes contraction in the x and y dimensions. v for most rocks is between 0.1 and 0.35 and for ice is typically 0.3–0.36.

Adding together the normal strains felt in each dimension from the stresses applied in all dimensions leads to the constitutive equations for normal stresses and strains:

$$\varepsilon_{xx} = \frac{1}{E}\sigma_{xx} - \frac{v}{E}\sigma_{yy} - \frac{v}{E}\sigma_{zz}$$

$$\varepsilon_{yy} = -\frac{v}{E}\sigma_{xx} + \frac{1}{E}\sigma_{yy} - \frac{v}{E}\sigma_{zz} \qquad (8.4)$$

$$\varepsilon_{zz} = -\frac{v}{E}\sigma_{xx} - \frac{v}{E}\sigma_{yy} + \frac{1}{E}\sigma_{zz}$$

Shear stresses lead to shear strains in the same directions, but not in orthogonal directions. The proportionality constant between shear stress and shear strain is called the *shear modulus* or *modulus of rigidity* (G_s), such that, for instance, $\sigma_{xy} = 2G_s\varepsilon_{xy}$. G_s can be rewritten in terms of

E and v: $2G_s = E/(1-v)$. Therefore, the constitutive relations for shear stresses and strains can be written as:

$$\varepsilon_{xy} = \frac{1+v}{E}\sigma_{xy}$$

$$\varepsilon_{xz} = \frac{1+v}{E}\sigma_{xz} \qquad (8.5)$$

$$\varepsilon_{yz} = \frac{1+v}{E}\sigma_{yz}$$

These three fundamental sets of relations (stress equilibrium equations, strain definition equations, and constitutive equations) provide the foundation for quantitatively investigating the mechanical behavior of geologic materials.

8.3 The Weight of the World: Isostasy and Flexure

An excess (or deficit of) mass in or on the lithosphere of a planetary body induces stress. The stress can be accommodated isostatically (by buoyancy in the asthenosphere) or flexurally (by the strength of the lithosphere). We will see that these two possibilities are actually end members of a continuum geophysical description.

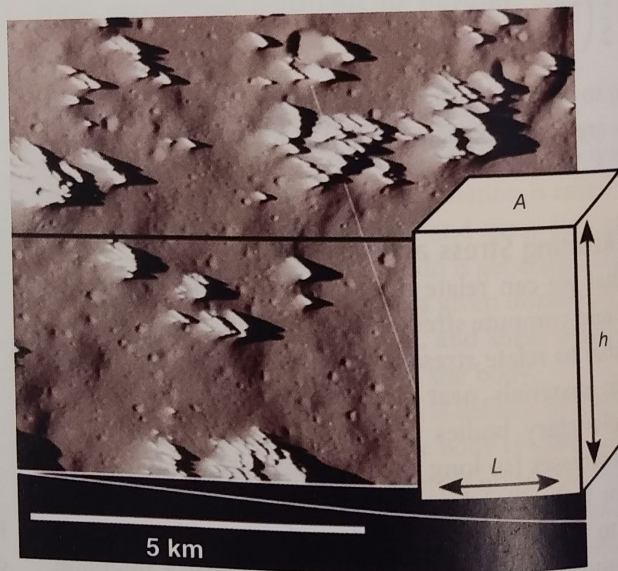### BOX 8.1 COMPRESSION OF ICE SPIRES ON CALLISTO

To illustrate a fairly straightforward application of the relations presented in this section, let's look at vertical erosional structures such as might occur from various processes throughout the Solar System. Figure 8.5 shows spires of ice on Callisto, one of Jupiter's large moons, resulting from long-term erosion of the surface. An idealized sketch for this problem is also shown.

We want to know how self-compression affects the dimensions of these features. If there is a significant effect on the dimensions, we would want to take the elastic response into account when studying further erosion. The two questions to answer are:

1. How much does the spire compress under its own weight?
2. How much extension ("bulging") occurs at the base from the weight?

The known dimensions and physical properties for this problem are: $\rho = 992$ kg/m³, $E = 9$ GPa, $v = 0.33$, $h = 500$ m, $L = 100$ m, and $g = 1.24$ m/s².

Figure 8.5 Image from NASA's *Galileo* mission shows spires of ice on Callisto. Inset shows an idealized sketch of an ice spire, showing variables used in Box 8.1.
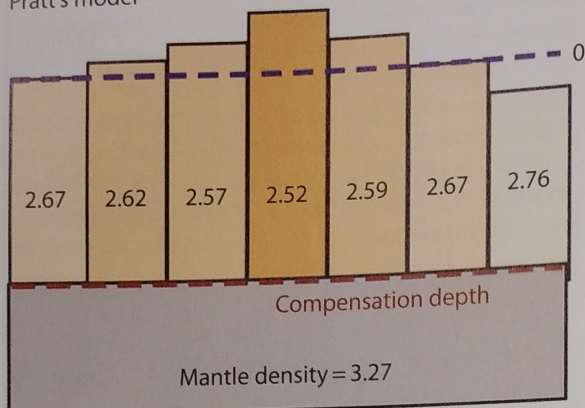
Looking at the problem as a whole reveals a path to take to the solution: The weight of the column will impose stresses, those stresses induce strains, and we can compute overall dimension changes from strains. The applied stress in the vertical (z) dimension is due to gravity, and there are no applied stresses in the horizontal (x and y) dimensions. From stress equilibrium
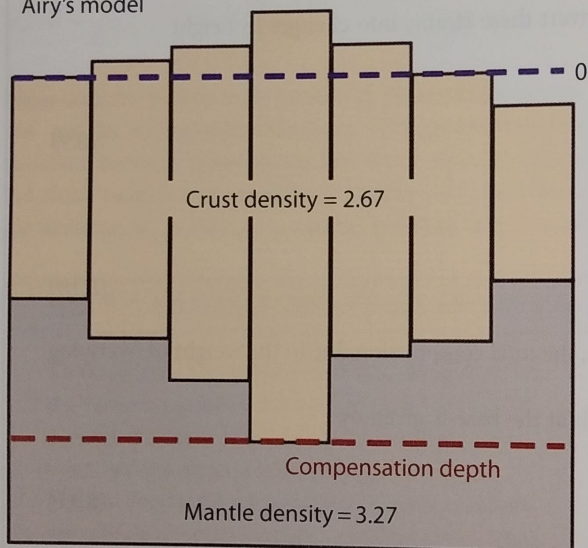
$$\frac{\partial \sigma_{zz}}{\partial z} = -\rho g \tag{8.6}$$

Solving for σ_{zz} by integration gives

$$\sigma_{zz}(z) = \int_h^z -\rho g \, dz = \rho g(h - z) \tag{8.7}$$

Since $\sigma_{xx} = \sigma_{yy} = 0$, the constitutive relations resolve to

$$
\begin{aligned}
\varepsilon_{xx} &= -\frac{v}{E}\sigma_{zz} = -\frac{v}{E}\rho g(h - z) \\
\varepsilon_{yy} &= -\frac{v}{E}\sigma_{zz} = -\frac{v}{E}\rho g(h - z) \\
\varepsilon_{zz} &= \frac{1}{E}\sigma_{zz} = \frac{1}{E}\rho g(h - z).
\end{aligned}
\tag{8.8}
$$

The strain definition equations provide the means to convert these strains into changes in height (h) and width (L):

$$\Delta h = \int_{\Delta h}^{0} du_z = \int_h^0 \varepsilon_{zz} dz = \int_h^0 \frac{1}{E}\rho g(h - z)dz \tag{8.9}$$

which gives

$$\Delta h = \frac{1}{2E}\rho g h^2 \tag{8.10}$$

For the properties and dimensions given for this problem, the total compression due to the weight of overlying ice is 1.7 cm.

Since $z = 0$ at the base of the spire, the change in width at the base is given by

$$\Delta L = \int_0^{\Delta L} du_x = \int_{-L/2}^{L/2} \varepsilon_{xx} dx = \int_{L/2}^{L/2} -\frac{v}{E}\rho g h \, dx \tag{8.11}$$

which gives

$$\Delta L = -\frac{v}{E}\rho g h L \tag{8.12}$$

For this problem, the "bulging" of the base amounts to 1.1 mm change (extension) in width. Similar geologic features, called buttes, occur in desert regions on Earth. For a typical butte with $h = 300$ m and $L = 75$ m (and ρ, E, and v appropriate for sandstone), Δh and ΔL are 2.4 cm and 1 mm, respectively, comparable to the values for ice spires on Callisto. Given the scale of the features, it would be safe to ignore the changing dimensions when studying further erosion.

8.3.1 Isostasy

The word **isostasy** comes from the Greek "iso" or equal and "stasis" or standing still, and it is a statement of buoyant equilibrium of lithospheric blocks. The basis of isostasy is the concept that any sufficiently large volume through the outer parts of a planetary body will have the same gravitational force as any other column of the same area and depth. This concept can be expressed mathematically, for a planar geometry, as

$$\sum_{i=1}^{N} \rho_{1,i} h_{1,i} = \sum_{j=0}^{M} \rho_{2,j} h_{2,j} = \text{constant} \tag{8.13}$$

where $\rho_{1,i}$ is the density of each layer of the first column, $h_{1,i}$ is the thickness of each layer in this column, and $\rho_{2,j}$ and $h_{2,j}$ are the densities and thicknesses of the layers in the second column. The summation extends to a sufficient depth – known as the compensation depth (D_c) – that the interior can be considered laterally

Pratt's model

| 2.67 | 2.62 | 2.57 | 2.52 | 2.59 | 2.67 | 2.76 |

Compensation depth

Mantle density = 3.27

Airy's model

Crust density = 2.67

Compensation depth

Mantle density = 3.27

Figure 8.6 The Pratt and Airy models of isostatic balance on a planetary body.

Figure 8.7 Schematic illustration of the flexure of an elastic plate in response to a downward forcing load, q_o. (a) shows the case of an intact plate, and (b) shows the case for a plate that is broken at $x = 0$. Note the forebulges some distance from the load where the plate bows up above the original horizontal. The position of the forebulge can be used to assess flexural properties (including thickness) of the plate. Modified from Turcotte and Schubert (2014).

theory to observed geomorphology is an effective means of determining physical properties of planetary surfaces.

Balancing forces and torques using the principles of Section 8.2 leads to a fourth-order differential equation that guides flexural response:
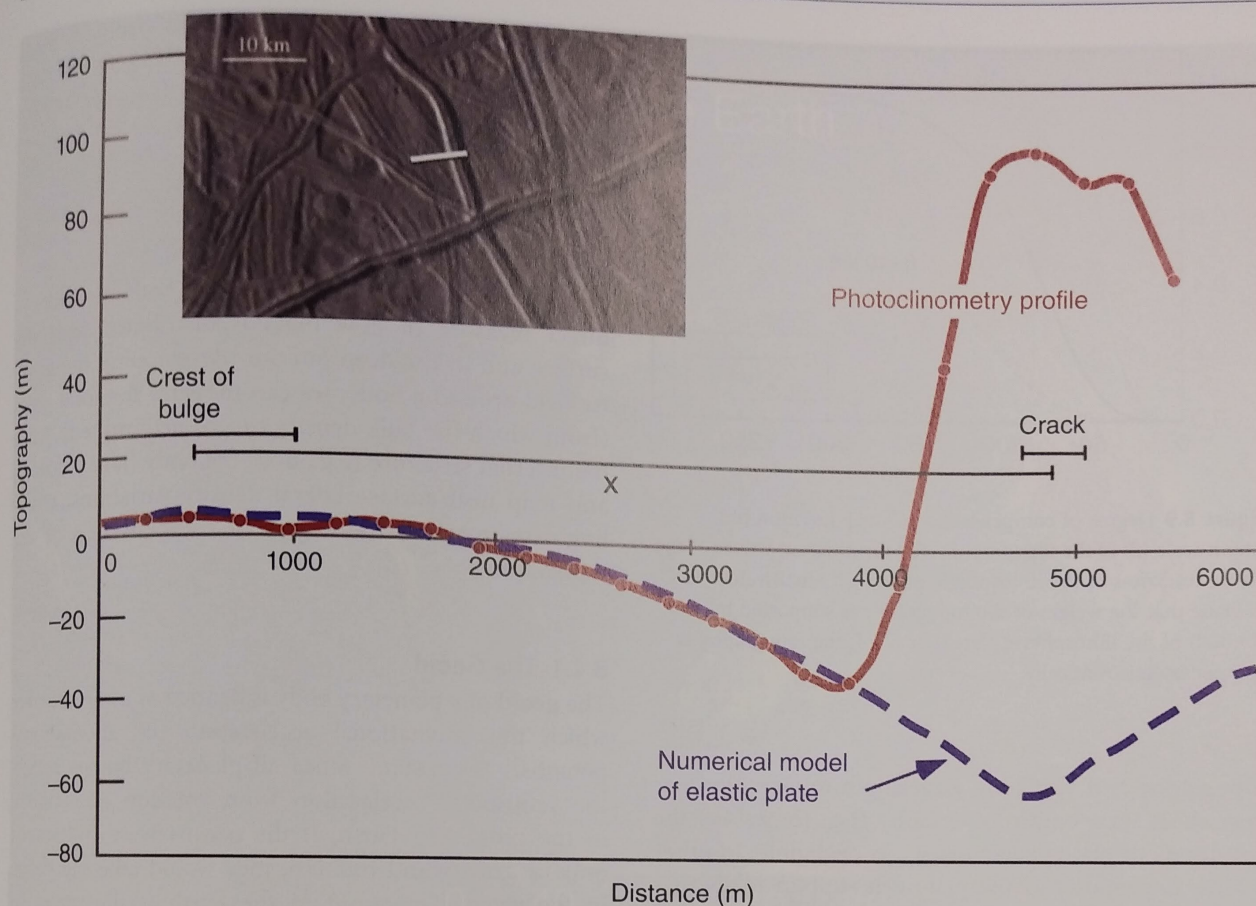
$$D\frac{d^4w}{dx^4} + P\frac{d^2w}{dx^2} + gw(\rho_m - \rho_{fill}) = q(x) \qquad (8.14)$$

This equation describes the vertical displacement, w, of the elastic lithosphere as a function of horizontal position, x. $q(x)$ represents the applied load, which can be a function of x, and P is any applied horizontal force. The third term on the left side represents the restoring force exerted by the fluid asthenosphere against the flexure: g is the acceleration of gravity, ρ_m is the density of mantle rock, and ρ_{fill} is the density of any material that is filling in the basin created by downward flexure of the plate (e.g., water in the ocean or sediments in a sedimentary basin). The mechanical properties of the plate are encapsulated in D, the flexural rigidity:

$$D = \frac{Eh^3}{12(1 - v^2)} \qquad (8.15)$$

with E and v as defined in Section 8.2 and h representing the elastic thickness of the plate. The solutions to Equation 8.14 depend on the details (boundary conditions) of the situation under consideration and quickly become complex enough to make it impossible to find analytic solutions. Nevertheless, two flexural problems are particularly useful to consider in a planetary context: loading on a plate and support of a periodic topographic load.

Consider a volcanic construct building up on a planetary surface, a plate being thrust on top of an adjacent block, or a ridge building up along a fissure. All of these processes lead to a load weighing down the elastic lithosphere. Figure 8.7 sketches the idealized flexural response

homogeneous. An assumption inherent in isostatic compensation is that the columns can be considered to be independent of each other – i.e., the crust is strengthless at the horizontal scale of the columns considered.

The equality can be achieved by lateral variations in crustal thickness, density, or both. The case of a topographic load on a constant-density crust being compensated by a thickening of the crust (i.e., a "root" extending into the mantle) is the *Airy model*. The case of compensation of a topographic load by lateral density variations is the *Pratt model* (Figure 8.6).

8.3.2 Flexure

Real materials have strength, and stress applied to a plate that is sufficiently strong will cause it to flex rather than to respond buoyantly. As illustrated in Figure 8.3, as long as the stress and strain are not too large, the flexural response can be treated elastically. Application of elastic flexure

Figure 8.8 Topographic profile perpendicular to a double ridge on Europa (solid red line) along with the modeled flexural plate profile (dashed blue line). The inset image shows the location of the profile. Hurford et al. (2005) used the distance between the center of the load and the crest of the flexural forebulge to estimate the thickness of the elastic plate. Modified from Hurford et al. (2005).

of a plate under a point or line load for the cases of an intact (a) or broken (b) plate. The solution of Equation 8.14 for an intact plate is

$$w = \frac{q_o \alpha^3}{8D} e^{-\frac{x}{\alpha}} \left(\cos \frac{x}{\alpha} + \sin \frac{x}{\alpha} \right) \qquad (8.16)$$

where q_o is the load, and α is the *flexural parameter*: $\alpha = [4D/(\rho_m - \rho_{fill})g]^{1/4}$. The solution for a broken plate is of a similar form:

$$w = \frac{q_o \alpha^3}{4D} e^{-\frac{x}{\alpha}} \cos \frac{x}{\alpha} \qquad (8.17)$$

These solutions reveal that the elastic plate will respond in a series of periodic highs and lows, with an amplitude that decreases exponentially with distance from the load. The distance to the first (largest) flexural high for an intact plate is $x_b = \pi\alpha$ and for a broken plate is $x_b = 3\pi\alpha/4$. We can infer the thickness of the elastic plate by measuring the horizontal distance from a surface load to the adjacent flexural rise.

This straightforward approach of inferring subsurface properties has been applied across the Solar System, from the Hawaiian islands on Earth, to scarps on Mercury and

Venus, to volcanic constructs on Mars, and to various ridges on icy moons and the dwarf planet Pluto in the outer Solar System (e.g., Barnett et al., 2002; Watters, 2003; Hammond et al., 2013; Huppert et al., 2015). Figure 8.8 shows results of such an analysis by Hurford et al. (2005) of double ridges on Europa. They found that Europa's elastic lithosphere at the time the ridges were emplaced was only a few hundred meters, compared to the tens of kilometers common for terrestrial planets.

In our second case, we'll consider periodic loading of a planetary surface, where the emplaced load is given by $q(x) = \rho_c g h_o \sin(2\pi x/\lambda)$. The topographic load is assumed to have the same density as the crustal plate, ρ_c, a topographic amplitude h_o, and wavelength λ. The flexural response of the underlying plate is constrained to have the same periodic response as the topography and can be expressed as

$$w = w_o \sin \frac{2\pi x}{\lambda}, \text{ where } w_o = \frac{\rho_c}{(\rho_m - \rho_c)} \frac{h_o}{\frac{1}{4}\left(\alpha\frac{2\pi}{\lambda}\right)^4 + 1} \qquad (8.18)$$

The most instructive aspect of this solution is to consider the extremes of very short wavelength
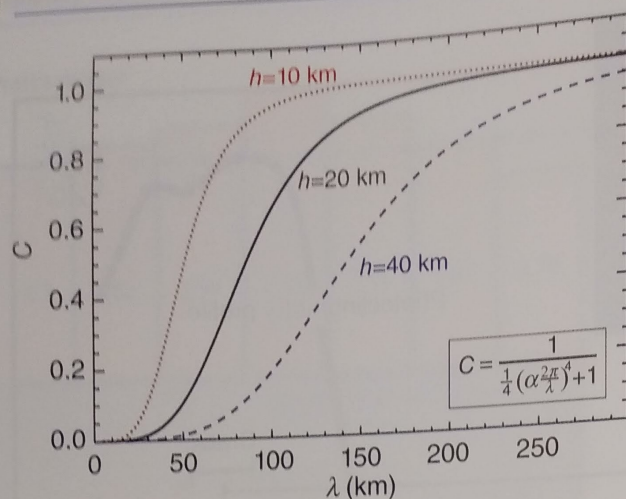
Figure 8.9 Degree of compensation (C) as a function of the length scale (λ) of the topographic load for different values of the elastic thickness of the lithospheric plate (h_e). Small values of C indicate that the weight of the topography is supported by the strength of the lithospheric plate. For $C \sim 1$, the topography is compensated isostatically.

topography and very long wavelength topography. For very short wavelength topography (i.e., for $\lambda \ll a$) the amplitude of plate deflection, w_o, is negligible. In other words, the rigidity of the plate can support loads that have a wavelength much smaller than the flexural parameter. For very long wavelength topography (i.e., $\lambda \gg a$), the solution simplifies to $w_o = \rho_c h_o / (\rho_m - \rho_c)$, which is the isostatic result! Figure 8.9 shows a plot of w_o divided by the isostatic result as a function of wavelength of the periodic load for different values of the elastic thickness (h in Equation 8.15) for a rocky body. Where this degree of compensation approaches 1, the load is supported isostatically, and where it is small, the topography is supported by the rigidity of the plate.

It is common for planetary bodies to exhibit cases of both end members of topographic support. For instance, gravity data (see Section 8.4) of Mars indicate that the southern highlands are in isostatic equilibrium with the northern lowlands. In other words, the lithosphere was not strong enough to support the topographic load when it was emplaced (very early in Mars' history). Using the Airy model, the measured topographic difference between the highlands and lowlands (~3 km), and assuming mantle and crustal densities of 3300 and 2900 kg/m^3, respectively, we find that the southern highland crust is approximately 24 km thicker than that of the northern lowlands. On the other hand, gravity data indicate that the much younger Tharsis volcanic plateau is not

isostatically compensated, so the lithosphere must have become much stronger (i.e., thicker) by the time the Tharsis volcanoes were emplaced (e.g., McGovern et al., 2002).

8.4 The Pull of Gravity

The gravity exerted by a planetary body provides a direct measure of how mass is distributed near the surface and in the deep interior. By mapping the gravity field around a body, we can measure the total mass (from which the bulk density can be determined), infer the internal structure (e.g., does the body have a core?), and map near-surface lateral density variations, enabling assessment of the degree of compensation of the topography.

8.4.1 The Geoid

The **geoid** of a planetary body is defined as a surface over which the gravitational acceleration (or gravitational potential) is constant. Since all planetary bodies rotate, the centripetal acceleration from rotation is included in the geoid. On Earth, if the oceans were influenced only by gravity and rotation, they would take the shape of the geoid. The geoid of the Earth is illustrated in Figure 8.10.

The concept of the geoid arises from Newton's law of gravity. The gravitational acceleration felt at any point external to a planetary body can be computed by:

$$g_m(r, \theta, \phi) = \int -G/\vec{b}^2 \, dm \tag{8.19}$$

where (r, θ, ϕ) are the body-centered coordinates of the external point, G is the universal gravitation constant, $\vec{b}$ is the vector between the infinitesimal mass unit (dm) and the external point, and the integral is throughout the body. For a perfect sphere, the solution of this integral has the relatively simple form

$$g_m(r, \theta, \phi) = -GM/r^2 \tag{8.20}$$

where $M = 4\pi \int_0^R \rho(r')r'^2 dr'$ is the total mass of the planetary body and r' is measured from the center of the body. The gravitational potential describes the work required to move a unit mass from infinity to a distance r from the center of the body. It is computed by $U = -GM/r$. $\int_\infty^r g_m \, dr$, which, for a sphere, becomes $U = -GM/r$.

Real planetary bodies, however, are not perfect spheres, and the solution for gravitational acceleration and gravitational potential can quickly become very complicated.

Geoid of the Earth

-80   -40   0   40   80
Geoid height (m)
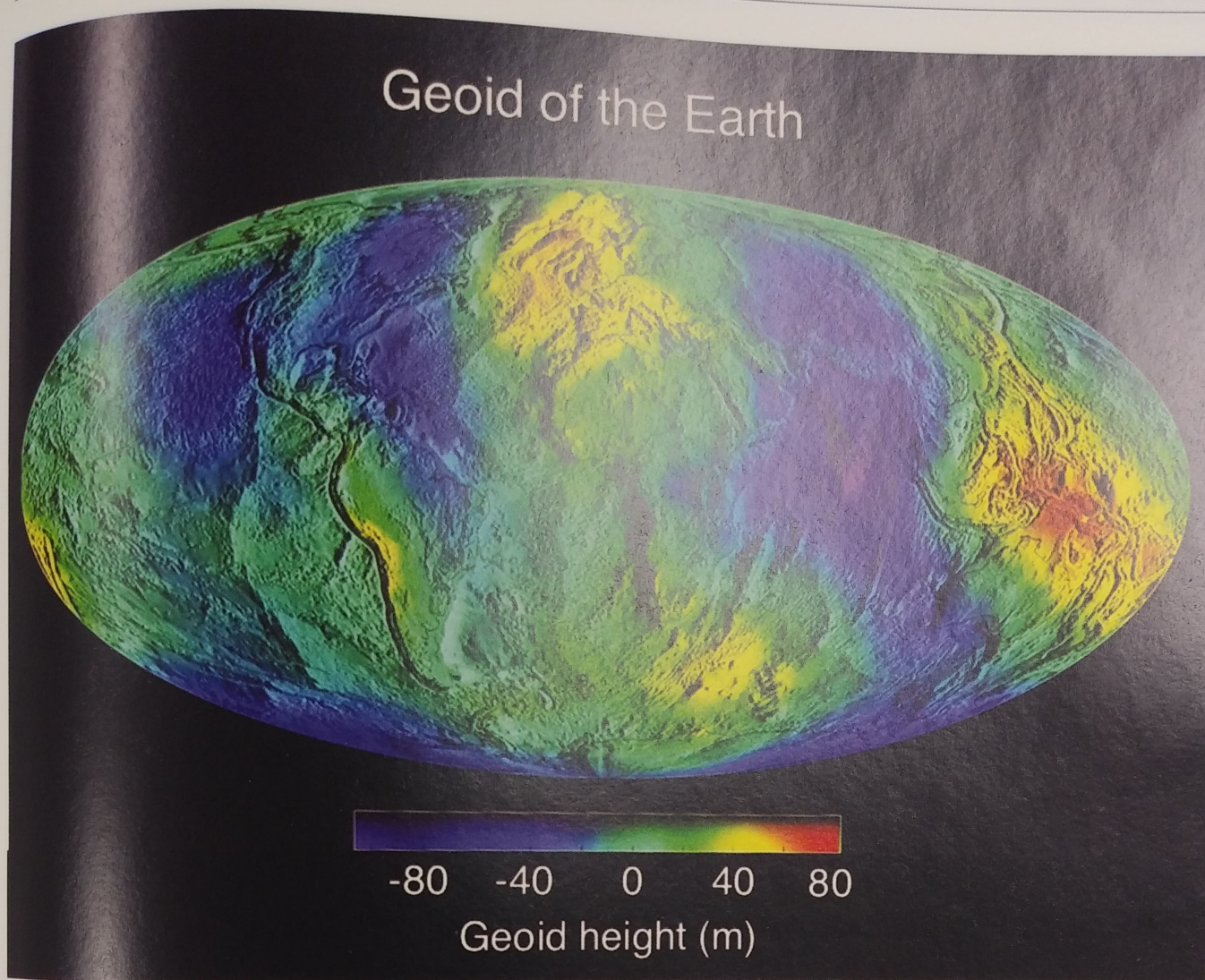
Figure 8.10 Geoid of the Earth. The deviations from a reference ellipsoid are quite small compared to the Earth's radius. Modified from delai.gsfc.nasa.gov.

To capture this complexity, gravitational potential is often expressed in terms of spherical harmonics:

$$U = -\frac{GM}{r} + \frac{GM}{r}\sum_{n=1}^{\infty}\left(\frac{R}{r}\right)^n J_n P_n^0(\sin\theta)$$

$$+\sum_{n=1}^{\infty}\sum_{m=1}^{n}\left(\frac{R}{r}\right)^n P_n^m(\sin\theta)(C_{n,m}\cos m\phi + S_{n,m}\sin m\phi)$$

$$(8.21)$$

In this expression, $P_n^m(\sin\theta)$ represents Legendre polynomials, and J_n, $C_{n,m}$, and $S_{n,m}$ are coefficients that describe the strength of the field at each value of n and m. The goal is to compute these coefficients from measurements of the gravity field for as many values of n and m as possible. Notice that the first term in Equation 8.21 is the spherical solution (corresponding to $n = m = 0$). The second term describes zonal harmonics – the case when $m = 0$ (note that $J_n \equiv C_{n,0}$). The zonal harmonics represent latitudinal gravity inhomogeneities. For example, J_2 describes the amount of rotational flattening (i.e., equatorial bulge) a body experiences from rotation. In the third term, the coefficients with $n = m$ are called *sectorial harmonics*, and these represent longitudinally symmetric inhomogeneities in the gravity field.

Higher degree and order (n and m) describe gravity signatures of ever decreasing size. In order to detect small-scale signatures, many gravity terms are required. The *EGM 2008* global gravity solution for the Earth goes to degree 2190 and order 2159, representing spatial scales of ~2 km). Thanks to NASA's *GRAIL* mission, the gravity field of the Moon is known to degree and order 900 (Lemoine et al., 2014). The higher degree and order terms fall off more quickly with distance from the body, making it very difficult to measure details of the gravity field from large distances.

8.4.2 Gravity Anomalies

Differences between a reference geoid and the measured gravity field are called **gravity anomalies**. The reference geoid for the Earth (World Geodetic System 1984; WGS84) is an ellipsoid of revolution with precisely defined coefficients. Anomalies in the gravity field arise from topography and from an excess or deficit of mass below the surface (i.e., lateral density inhomogeneities) (Figure 8.11). Gravity measurements on Earth have traditionally been made using a gravimeter (a very sensitive accelerometer). In modern times, tracking satellites as they move through Earth's gravity field has provided more consistent, detailed datasets. Similarly, tracking spacecraft as they perform flybys or orbit other planetary bodies provides gravity measurements across the Solar System. The *GRAIL* mission precisely monitored the distance between two spacecraft (*Ebb* and *Flow*) to make detailed measurements of the Moon's gravity field (Zuber et al., 2013).

Gravity data are often reported after one or both of two important corrections are made. The *free air correction* adjusts the data for the elevation or altitude of the measurement above the reference geoid, assuming there is no mass (i.e., just free air) between the instrument and the reference geoid. In other words, any mass from topography is ignored. The *Bouguer correction*, on the other hand, specifically adjusts for the mass of known topography between the measurement and the reference geoid. Since surface topography can be observed, the Bouguer correction highlights subsurface mass variations. Figure 8.12 shows a gravity map of the Moon from *GRAIL*. The large anomalies associated with the lunar maria reveal significant excess mass below those impact basins, providing critical constraints on formation models.

8.4.3 Assessing the Compensation State

If the topography is compensated (e.g., by a root in the Airy model), no anomaly will show up in the free air correction. If the topography is not compensated (e.g., if it is supported by the strength of the lithosphere), a positive gravity anomaly will show up. Isostatically compensated elevated terrain will show up as a gravity low after the Bouguer correction, since the root has a lower density than the surrounding mantle, whereas flexurally supported terrain will not show a Bouguer anomaly (Figure 8.11).

In Section 8.3, we computed the flexural response of an elastic plate to periodic topography of the form $q(x) = \rho_c g h_o \sin(2\pi i/\lambda)$, and we noted that short wavelength (i.e.,
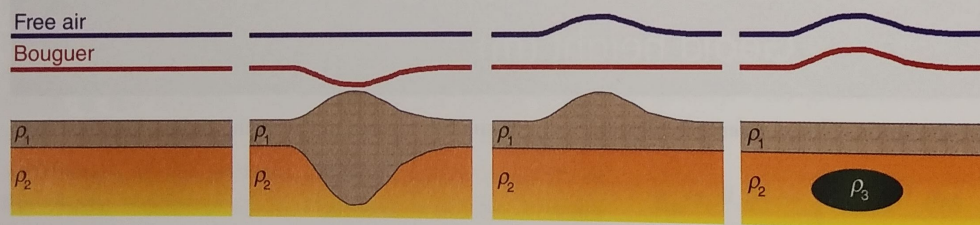
Figure 8.11 Illustration of gravity profiles after free air (blue) and Bouguer (red) corrections. In all frames $\rho_1 < \rho_2 < \rho_3$. (a) If there are no topography or lateral density variations, both gravity profiles are flat. (b) Compensated topography has no free air anomaly, but has a negative Bouguer anomaly. (c) Topography that is not compensated (i.e., is supported by the strength of the lithosphere) shows a positive free air anomaly, but no Bouguer anomaly. (d) A buried mass excess has a positive anomaly with both corrections.
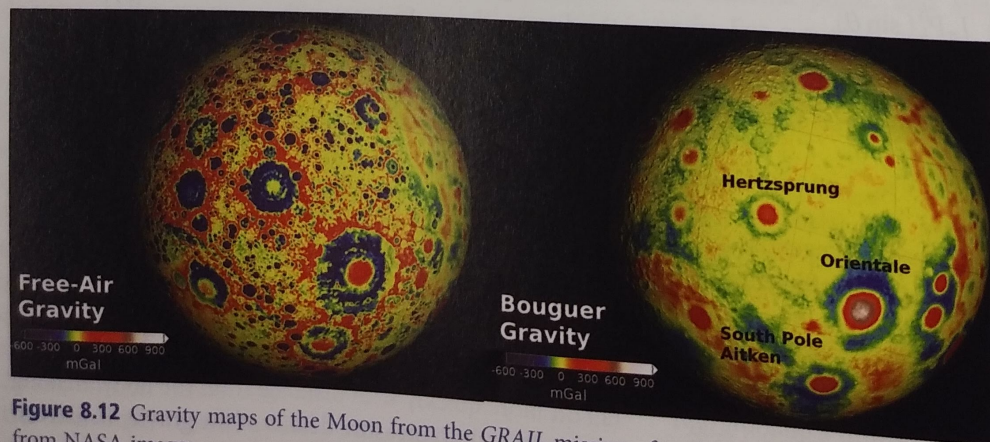
Figure 8.12 Gravity maps of the Moon from the *GRAIL* mission after free air and Bouguer corrections have been applied. Modified from NASA images.

(a) Earth

h = 28.4 km

(b) Venus

h = 33 km
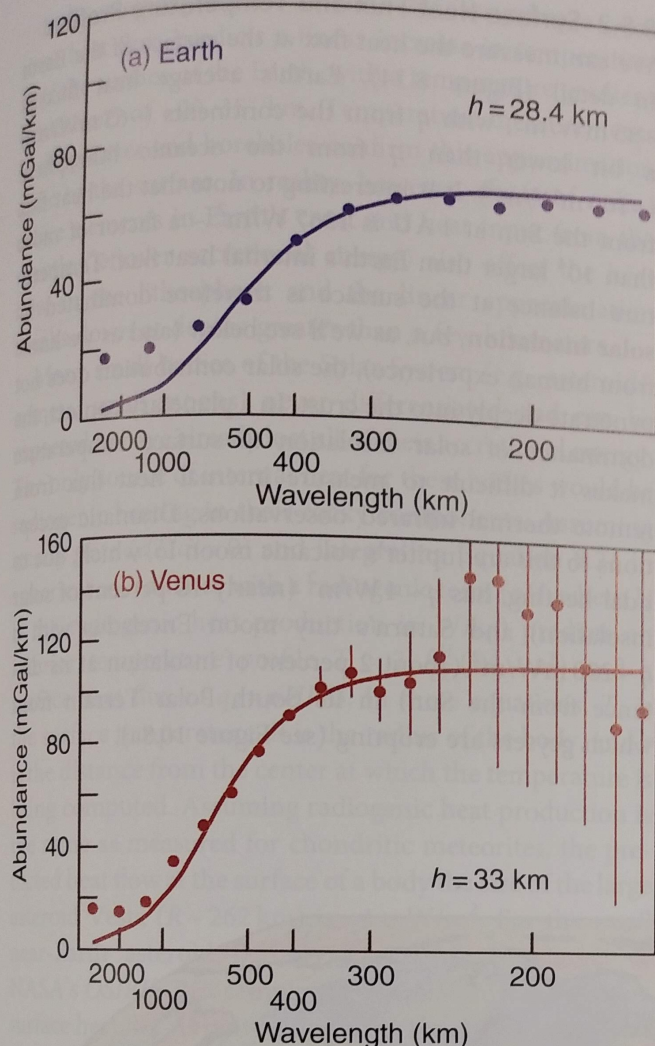
Figure 8.13 Admittance measurements (data points) for regions on the Earth (Hawaii) and Venus (Ulfrun) indicate similar elastic lithosphere thickness on the two bodies. The solid lines are model fits to the data. Modified from Nimmo and McKenzie (1998).

small-scale) topography can be supported by the strength of the plate and long wavelength topography is isostatically compensated. It turns out that the gravity anomaly produced from that topography and the resulting lithospheric deflection is

$$\Delta g_B = \frac{-2\pi\rho_c G}{1+\frac{1}{4}\left(\alpha\frac{2\pi}{\lambda}\right)^4} e^{-\frac{2\pi z}{\lambda}} h_o \sin\frac{2\pi x}{\lambda} \tag{8.22}$$

Equation 8.22 has two important attributes to note. The first is that, once the topography is divided out, the gravity anomaly has the same form as the degree of compensation plotted in Figure 8.9. The ratio of gravity to topography is called **admittance**. Figure 8.13 shows plots of admittance for Venus and the Earth, illustrating the power of combining measurements of gravity and

topography to assess the elastic thickness on a planetary surface. The second is that the gravity anomaly signature falls off exponentially with altitude and with decreasing wavelength of topography; small-scale gravity anomalies are difficult to detect from large distances.

8.5 Conductive Heat Flow

As we learned in Chapter 6, the transfer of heat is an important driver of many geologic processes throughout the Solar System. Of the three methods of transferring heat (conduction, convection, radiation), conduction is by far the most important in the solid outer layers of planetary bodies with which we interact. The crustal layer of a body is heated and cooled from the top by radiation and may have heat delivered to the bottom through convection, but the thermal energy makes its way through the crust by conduction. The efficiency of conductive versus convective heat transport therefore controls the interior temperature. We can exploit our knowledge of heat conduction to remotely infer surface properties from remote thermal infrared observations. Fracturing of surface rocks from stresses imposed by cyclical heating and cooling has recently been recognized as a potentially important mechanism for breaking down rocks and building regolith on many planetary surfaces.

8.5.1 Fourier's Law and Heat Diffusion

Jean-Baptiste Joseph Fourier, like other famous early scientists, was interested in a wide variety of topics, both natural and philosophical. Fourier made significant advances in understanding heat flow by combining experimentation, mathematical advances, and by breaking his thought from the paradigm of action-at-a-distance, which had been prevalent at the time, reinforced by Newton's brilliant development of the law of gravity. Fourier noted that the flux of heat (energy per time per area flowing through a surface) is directly proportional to the temperature difference immediately on either side of the surface. From this observation, he developed the partial differential equation governing heat flow that now bears the name Fourier's Law:

$$q_z = -k\frac{\partial T}{\partial z} \tag{8.23}$$

or, in three-dimensional vector notation,

$$\vec{q} = -k\vec{\nabla}T \tag{8.24}$$

In these equations, q is the heat flux (SI units of W/m^2), T is temperature, and k is the thermal conductivity (units of W/m/K). The thermal conductivity describes the amount

of energy that can be transported a given distance for a given ΔT. It is typically in the range of 1–4 W/m/K for rocks and ice and 10–80 W/m/K for metals.

A mass of material can store heat as well as conduct it. Conservation of internal energy including both heat storage and conduction adds a time component and leads to the law of heat diffusion:

$$\frac{\partial T}{\partial t} = -\frac{k}{\rho c_p}\frac{\partial^2 T}{\partial z^2} \tag{8.25}$$

or in three-dimensional vector notation

$$\frac{\partial T}{\partial t} = -\frac{k}{\rho c_p}\nabla^2 T \tag{8.26}$$

Here, ρ is density and c_p is the specific heat capacity, which describes the amount of energy required to change the temperature of 1 kg of material by 1 K (units of J/kg/K), and k is assumed to be constant. If there are other energy sources or sinks (e.g., radiogenic heat production), they can be included as additional terms to this equation. The quantity $k/\rho c_p$ is known as the thermal diffusivity (κ; units of m^2/s).

8.5.2 Surface Heat Flux and Temperature Profiles

We can measure the heat flux at the surface of the Earth in detail (Figure 8.14). Earth's average heat flux is $\sim$85 mW/m^2, with q from the continents ($\sim$65 mW/m^2) a bit lower than q from the oceanic lithosphere ($\sim$100 mW/m^2). It is interesting to note that the heat flux from the Sun at 1 AU is 1367 W/m^2 – a factor of more than 10^4 larger than Earth's internal heat flux. Temperature balance at the surface is therefore dominated by **solar insolation**, but, as we'll see below (and as we know from human experience), the solar contribution does not penetrate deeply into the crust. In a planetary context, the dominance of solar insolation to surface temperature makes it difficult to measure internal heat flux from remote thermal infrared observations. Dramatic exceptions to this are Jupiter's volcanic moon Io, which, due to tidal heating, has $q \sim 4$ W/m^2 (nearly 10 percent of solar insolation) and Saturn's tiny moon Enceladus with a $q \sim 250$ mW/m^2 (about 2 percent of insolation at its distance from the Sun) in its South Polar Terrain from which geysers are erupting (see Figure 10.8a).
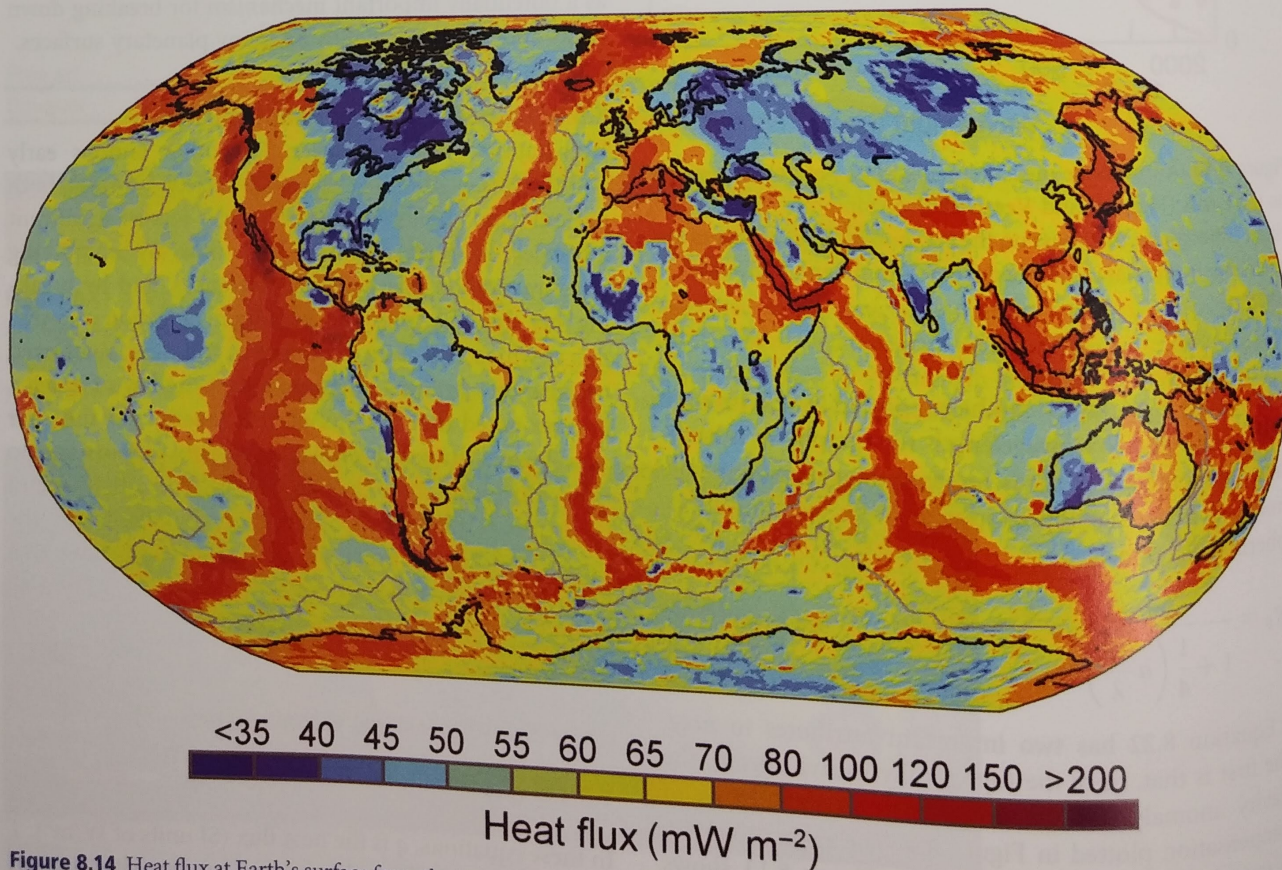
Figure 8.14 Heat flux at Earth's surface from the interior. Actual heat flow measurements are fairly sparse over much of Earth, and the map has been constructed by incorporating multiple geological and geophysical proxies of heat flow. Modified from Goutorbe et al. (2011).

Integrating Equation 8.23 (or 8.24), assuming a constant heat flux, predicts a linear increase in temperature near the surface of the Earth, with a temperature gradient (geotherm) of ~20–35°/km. Temperature measurements in deep caves and boreholes confirm this approximation close to the surface. In reality, however, decay of radioactive elements in Earth's crust and heat input from the mantle (leftover accretional energy) also affect the heat flow in the lithosphere, and the linear approximation breaks down at depths greater than a few kilometers.

Many small bodies of the Solar System (e.g., asteroids, comets, small moons) never differentiated and can be expected to have already lost all of their accretional energy. The only source of internal heat for these bodies would be radiogenic heating in their rocky components. Assuming steady state ($dT/dt = 0$) and integrating Equation 8.24 in spherical coordinates with a radiogenic term (ρH, where H is the radiogenic heat production in W/kg) predicts an interior temperature profile $T = T_o \frac{\rho H}{6k}(R^2 - r^2)$ and a surface heat flux of $q_o = \rho H R/3$. In these equations, T_o is the surface temperature, R is the radius of the body, and r is the distance from the center at which the temperature is being computed. Assuming radiogenic heat production is the same as measured for chondritic meteorites, the predicted heat flow at the surface of a body the size of the large asteroid Vesta ($R \sim 262$ km) is ~1 mW/m². For the small near-Earth asteroid Bennu ($R \sim 250$ m), the target of NASA's *OSIRIS-REx* sample return mission, the predicted surface heat flow is only ~1 μW/m². These very small heat fluxes would be nearly impossible to distinguish from solar heating in remote observations.

8.5.3 Solar Heating

As mentioned above, the thermal energy balance near the surface of planetary bodies is dominated by solar insolation. Since planetary bodies rotate, the solar energy input could be (loosely) approximated as a time-varying periodic surface temperature: $T_o = \Delta T \cos(\omega t)$, where ΔT is the amplitude of the temperature variation and ω is the rate of variation (i.e., rotation rate). This assumption is oversimplified, but has the virtue of being analytically solvable. Integrating Equation 8.25 with this surface temperature boundary condition gives for the temperature as a function of depth and time:

$$T(z,t) = T_o + \Delta T e^{-\sqrt{\frac{\omega \rho c_p}{2k}}z} \cos\left(\omega t - \sqrt{\frac{\omega \rho c_p}{2k}}z\right)$$

(8.27)

This solution illustrates two important aspects of solar-driven temperature variations: the temperature variation falls off exponentially with depth, and there is a time

(phase) delay between the surface and subsurface temperature cycles. The depth at which ΔT falls off by a factor of $1/e$ is called the *thermal skin depth*, and is given by

$$d_s = \sqrt{\frac{2k}{\omega \rho c_p}}$$

(8.28)

The diurnal thermal skin depth for Earth is between about 5 and 20 cm, depending on the soil properties. The annual thermal skin depth, due to changing seasons, for Earth is about 1–4 m.

In reality, solar heating is not perfectly sinusoidal – there is no solar heat input during night time. In this case, the effective surface boundary condition is on heat flux, not temperature. Flux (energy) balance at the surface can be expressed as

$$\frac{S_o}{r_{AU}^2}(1 - A_B)\cos\theta_i - k\frac{\partial T}{\partial z}\bigg|_{surf} - \epsilon\sigma_B T_o^4 = 0$$

(8.29)

where S_o is the solar flux at 1 AU (1367 W/m²), r_{AU} is the heliocentric distance in AU, A_B is the Bond albedo, θ_i is the solar incidence angle of the surface facet considered, ϵ is the bolometric emissivity, and T_o is the surface temperature. If the specific situation includes other heat sources or sinks (e.g., heating from the atmosphere, volatile sublimation), extra terms can be added. With this boundary condition, Equation 8.25 is no longer solvable analytically – numerical techniques are necessary. Figure 8.15 illustrates temperature versus depths curves for a model surface. Note the decrease in amplitude of temperature variations and phase offset of the temperature wave with depth.

Another parameter that arises from considerations of heat conduction is **thermal inertia**:

$$\Gamma = \sqrt{k\rho c_p}$$

(8.30)

where Γ describes a material's resistance to changes in temperature and has the somewhat cumbersome units of J/m²/K/s$^{1/2}$. Thermal inertia is often used as a proxy for grain size, as described in Section 2.5.4. Small grains (e.g., sand and dust) have low thermal inertias – they heat up and cool down quickly (e.g., the Moon has $\Gamma \sim 50$ in these units). Large grains and bedrock, on the other hand, take a longer time to heat up and cool down. Observations of temperature as a function of time of day can be used to determine thermal inertia. Figure 8.16a shows diurnal temperature curves for surfaces with different thermal inertias. Figure 8.16b plots thermal inertias of asteroids versus their diameters, indicating that large asteroids are covered in fine-grained regolith material, whereas the surfaces of small asteroids appear to be, on average, blockier.
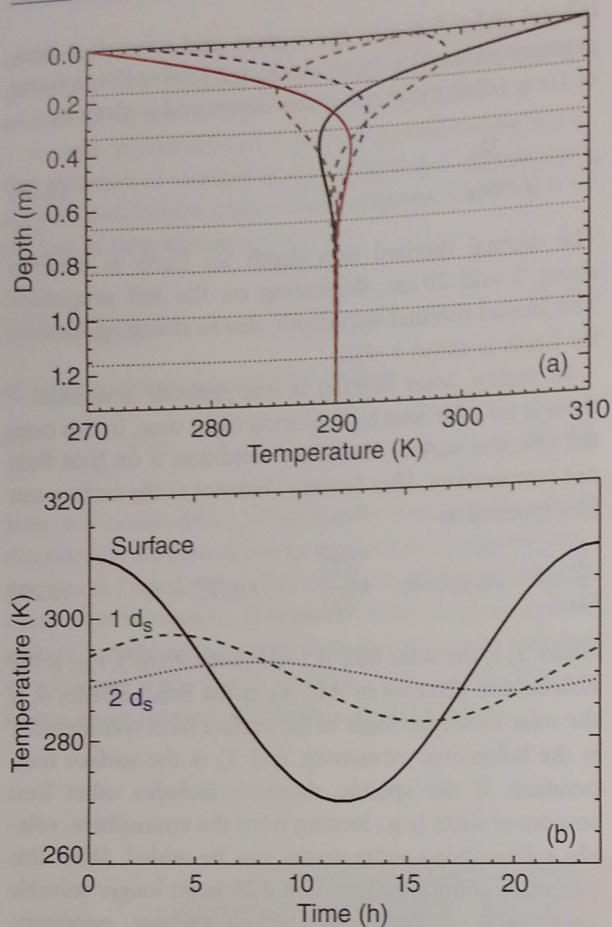
Figure 8.15 Example temperature profiles from Equation 8.27 for a planetary body at 1 AU with a rotation period of 24 h and thermal diffusivity of 10^{-6} m²/s. (a) Temperature variation with depth at different times of day. The horizontal dotted lines mark intervals of skin depth down to eight skin depths below the surface. The temperature varies by 40 K at the surface, but that amplitude of temperature variation quickly diminishes, and by five skin depths almost no temperature variation is apparent. The plot also illustrates that the temperature gradient, which is proportional to heat flux (Equation 8.23), changes over the course of the day, so that heat is conducted into the surface in the daytime and out of the surface at night time. (b) The sinusoidal temperature variation assumed in this simple model at the surface and at one and two skin depths below the surface. The diminishing amplitude of the temperature variation is again apparent, as is the changing phase of the temperature variation – the peak temperature moves from 0 h (noon) at the surface to ~4 h at $1d_s$ and ~8 h at $2d_s$.

8.5.4 Thermal Stresses

Heating and cooling of geologic materials leads to expansion and contraction within the material. The strains of expansion and contraction lead, by the constitutive relations of Equations 8.5 and 8.6, to stresses within the material. The amount of strain experienced is described by the thermal expansion coefficient (α): $\varepsilon = \alpha \Delta T$. On Earth,
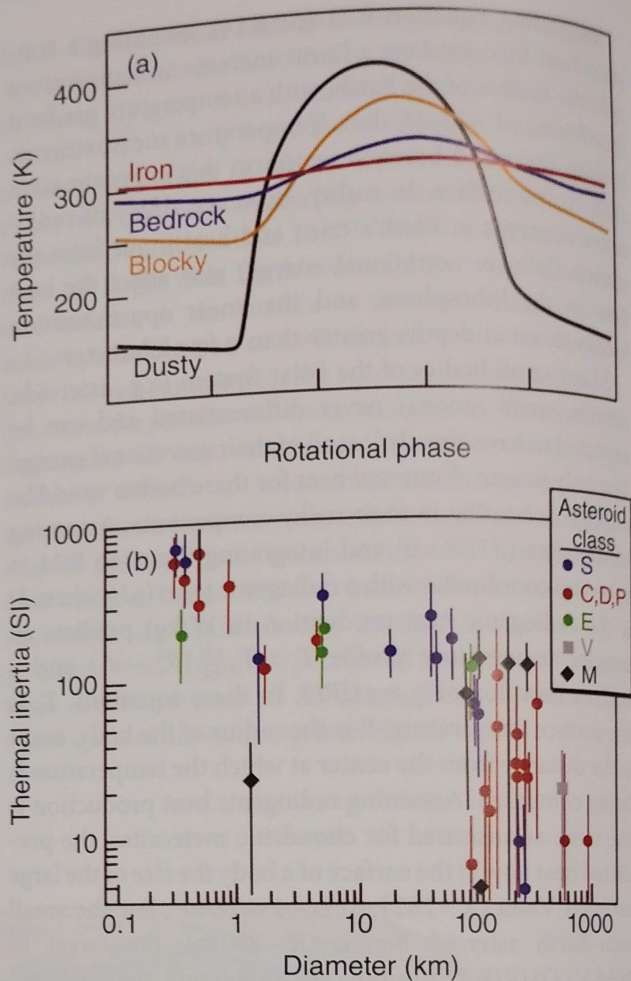
Figure 8.16 (a) Surface diurnal temperature curves for bodies of different surface types, and therefore thermal inertias. These profiles are computed with a thermophysical model that uses the surface energy balance given in Equation 8.29. Measuring temperatures of a surface at different times of day is a powerful means of determining the thermal inertia of a surface. (b) Thermal inertias of asteroids as a function of diameter. The letters in the key are different asteroid spectral types (which correspond to different inferred compositions). Modified from Delbó et al., (2015).

thermal stresses have long been recognized as a mechanism for spalling of material off of rocks at the surface. Airless planetary bodies (e.g., Mercury, asteroids, comets) can experience even more dramatic temperature variations, and recent thermal cycling experiments on meteorites suggest that thermal fragmentation of surface rocks could, in some cases, surpass impacts as a primary mechanism to form regoliths on these surfaces (Delbó et al., 2014).

8.6 Going with the Flow: Fluid Mechanics

Many processes in planetary science involve the flow of fluids. Fluvial and aeolian processes, those involving flowing liquid and air at the surface of a planetary body,

Table 8.1 Viscosities for some common materials

Material	μ (Pa·s)
Air	1.8×10^{-5}
N_2 (liquid)	1.5×10^{-4}
H_2O (liquid)	9×10^{-4}
Oil (motor, olive)	~ 0.1
Basaltic, andesitic, rhyolitic lava	$\sim 10^4, 10^7, 10^{11}$
H_2O (ice, 273 K)	$\sim 10^{14}$
Earth's mantle	$\sim 10^{21}$

are covered in detail in Chapters 13 and 14. In this chapter, we focus on the flow of mantle rocks.

A fluid can be defined as a material that deforms continuously under an applied stress. We discussed in Section 8.2 the response of an elastic solid to an applied stress – it will deform (i.e., rearrange its structure at the microscopic level) until it balances the applied stress. For small stresses in most geologic solids, the elastic response is linear ($\sigma = E\varepsilon$). Fluids, however, are never able to balance the stress – their molecules keep slipping past one another. In this case, the applied stress leads to a continuous rate of deformation, or a **strain rate** ($\dot{\varepsilon} = d\varepsilon/dt$; the dot indicates differentiation with respect to time). For many geologic fluids, the relationship between σ and $\dot{\varepsilon}$ is linear; such materials are called Newtonian fluids:

$$\sigma = \mu\dot{\varepsilon} \tag{8.31}$$

The proportionality constant between stress and strain rate is the dynamic viscosity (μ), which has units of Pa·s. Dynamic viscosity describes the stress required to cause a given strain rate in a fluid. Dividing μ by the density of the fluid gives a quantity called the kinematic viscosity (ν), which has units of m^2/s. Recall that these are the same units as thermal diffusivity, and ν similarly characterizes the diffusivity of momentum in a fluid. But here, we will work with the dynamic viscosity, μ. The viscosity spans many orders of magnitude for geologic materials, and we'll see in Section 8.7 that for a given material it depends strongly on temperature, grain size, and in some instances even on the applied stress. Table 8.1 lists typical viscosities for some common materials.

8.6.1 Conservation Laws
Analyses of fluid mechanics problems use the principles of conservation of mass, momentum (i.e., force balance), and energy. Here, we'll focus on mass and momentum conservation. If we think about a small volume in a flow, the conservation of mass is a statement that no mass can be gained or lost from the volume. Any mass leaving the volume must be replaced by new material entering the volume, at the same rate. Similarly, any change in density of the material within the volume must be balanced

by material entering or leaving the volume. Considering flow in just one dimension, this conservation law is expressed as

$$\frac{\partial \rho}{\partial t} + \frac{\partial (\rho v_x)}{\partial x} = 0 \tag{8.32}$$

where v_x is the velocity of flow in the x direction.

Conservation of momentum looks at force balance on all sides of the same small volume, including pressure gradients in the flow and buoyancy of the volume relative to the surrounding fluid. The resulting relationship is called the *Navier–Stokes* equation, which with flow in one dimension is

$$\rho\left[\frac{\partial v_x}{\partial t} + v_x \frac{\partial v_x}{\partial x}\right] = \mu \frac{\partial^2 v_x}{\partial z^2} - \frac{\partial P}{\partial x} + \Delta\rho g \tag{8.33}$$

It is useful to look into the physical meaning of each term in the Navier–Stokes equation. The first term on the left side considers how the flow is changing with time (it is zero if flow is constant). The second term characterizes the inertia of the flow; this is the term in which turbulence enters (the term is small if the flow is smooth or laminar). The first term on the right side controls how sluggish the flow is, or how easily momentum is diffused across the flow. The second term describes pressure gradients along the flow, which can help or hinder flow. The last term represents the buoyancy relative to the surrounding flow and should only be included if a component of the flow is along the direction of gravity.

8.6.2 Relaxing Topography
When a load is added to or removed from the lithosphere, the lithosphere bends and the asthenosphere flows to achieve an isostatic balance. The best-known example of this process on Earth is post-glacial rebound. During the last ice age, great sheets of ice weighed down the lithosphere, flexing it into the asthenosphere. Ever since that ice melted, the fluid-restoring force of the asthenosphere has been pushing the lithosphere back into place.

Because the rebound is controlled by the viscous flow of the mantle, Equation 8.33 can be solved to describe the subsequent isostatic rebound of the surface. The full solution combines the flexural response of the lithosphere and the fluid response of the asthenosphere and is generally done numerically. Nevertheless, it has been shown that the vertical displacement (w) of the topography recovers with an exponential timescale:

$$w = w_o e^{-\frac{t}{\tau}}, \quad \text{where } \tau \approx \frac{4\pi\mu}{\rho g L} \tag{8.34}$$

Here, w_o is the original vertical displacement, and L is the horizontal length of the original load. This solution holds

for the common case of $w \ll L$. By dating paleo-shorelines (i.e., elevated beaches) since the end of the ice age, geologists have been able to determine the timescale of rebound and, from that, estimate the viscosity of the asthenosphere (Figure 8.17).

On other planetary bodies, impacts act to remove mass very quickly from the lithosphere, leaving craters. These craters undergo isostatic rebound as well. In some cases, particularly on icy bodies, the craters can relax completely, so that no negative topography is left. Because the crater rims have a much shorter horizontal length scale, the crater rims still often rise above the surface after the crater itself has completely rebounded (e.g., Ganymede in Figure 8.17). Images of the surface of the dwarf planet Ceres (diameter ~960 km) from the *Dawn* mission revealed large impact craters that had rebounded. This observation is a clear indication that Ceres has, or at least had for some period of time after the large craters formed, a ductile asthenosphere.

As we'll see in Section 8.7, viscosity is a strong function of temperature. As temperature increases, viscosity decreases, and topography relaxes more quickly. Crater relaxation can therefore be used to uncover changes in heat flow within a planetary body. Enceladus is an excellent example. As will be described in Section 9.5.3, the south pole of Enceladus contains tectonic fractures with high heat flow, but other parts of the surface are geologically old, as evidenced by high densities of impact craters. Many of these craters, it turns out, have experienced significant amounts (up to 90 percent) of relaxation. Numerical modeling of the process by Bland et al. (2012) indicates that heat flows comparable to that occurring at the south pole must have occurred in these other regions at some time in Enceladus' past.

8.6.3 Convection

A fluid layer heated from below and cooled from the top (a common occurrence in planetary bodies radiating their heat to space from their surfaces) is gravitationally unstable. The hot fluid at the base is less dense due to thermal expansion, and it therefore wants to rise buoyantly. Viscous forces in the fluid layer fight against this buoyancy; convection can only occur if the buoyancy force is larger than the viscous forces.

Mathematically, the thermal buoyancy is included in the buoyancy term in the Navier–Stokes equation (Equation 8.33). The change in density driving the buoyancy is controlled by the thermal expansion coefficient and the temperature. In other words, inclusion of thermal buoyancy adds a temperature term to the Navier–Stokes equation. The temperature is solved using the heat diffusion equation (Equation 8.25), but a term must be added to that equation as well. As the hot parcel rises, it carries heat with it – heat is being transported directly by the movement of the fluid. This *advection* adds a term that includes velocity to the heat diffusion equation. The appearance of temperature in the flow equation and velocity in the heat equation requires both to be solved simultaneously to investigate convection. This coupling makes quantitative studies of convection difficult, requiring numerical techniques.

To examine the conditions under which convection gets started, it is useful to define a parameter called the *Rayleigh number*. The Rayleigh number compares the thermal diffusion timescale across the layer to the timescale for the warm fluid to move through the layer and is given by

$$Ra = \frac{g\rho_o \alpha_v (T_1 - T_0) b^3}{\kappa \mu} \tag{8.35}$$

Here, ρ_o is the standard density of the fluid (before heating), α_v is the volumetric thermal expansion coefficient, T_1 and T_0 are the temperatures at the base and top of the layer, respectively, κ is the thermal diffusivity, and b is the thickness of the layer. Convection can get started if Ra is greater than some critical value that depends strongly on whether the top layer is free to move horizontally (mobile lid) or is fixed in place (stagnant lid) (see Chapter 9 for more detail).

Convection cells can be envisioned somewhat like a conveyer belt, with warm fluid rising, moving horizontally while it cools to the surface, and the cool fluid falling back down. The horizontal motion imposes a stress on the (typically rheologically brittle) surface. If the stress on the lithosphere from convection is larger than its strength, the lithosphere will break, and the resulting plates can be moved by the convection conveyer. On the other hand, if the lithosphere is strong enough to withstand convective stresses, it will remain intact and will not move. As we know, the Earth's lithosphere is broken into tectonic plates that move and subduct along with the convection cells. No other planetary bodies are known to support plate tectonics; their lithospheres are apparently strong enough to withstand the stresses of the convection roiling beneath the surfaces.

8.7 Rheology

In this chapter, we have introduced several of the more common processes that geodynamicists investigate. For each process, we have made some assumptions about how geologic materials behave under stress. We have treated rocks as solid materials that respond in a linear, elastic way to stress – deformation is instantaneous, recoverable when the stress is removed, and scales
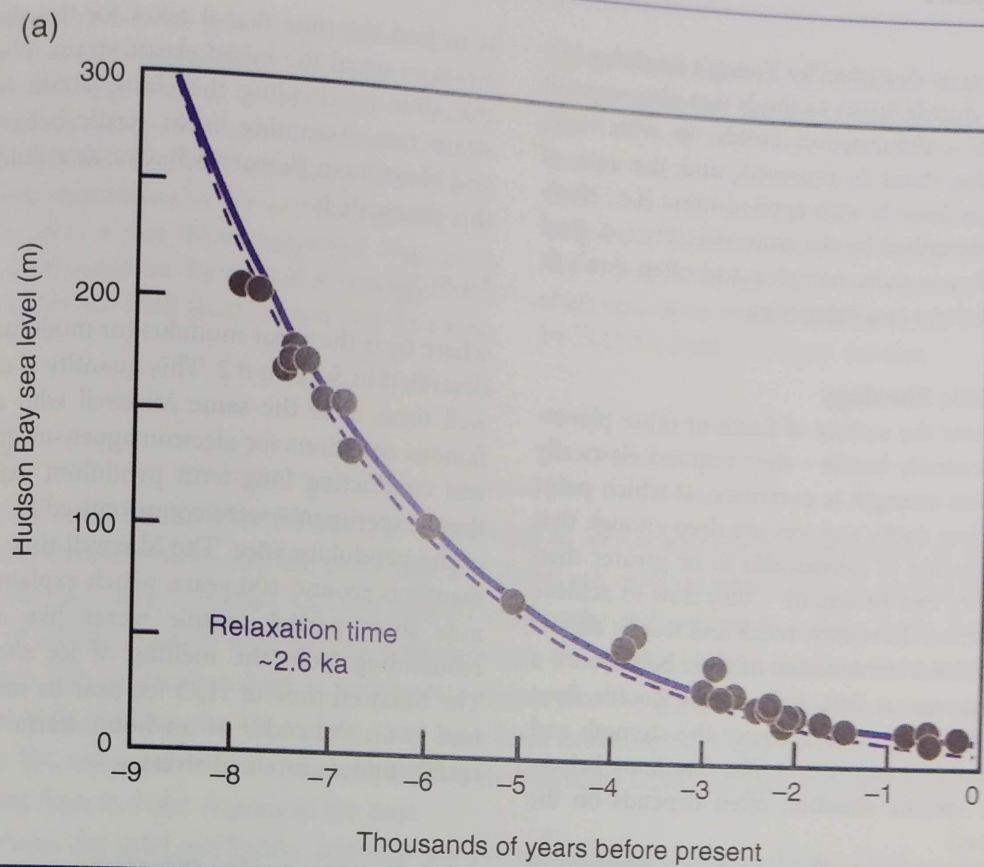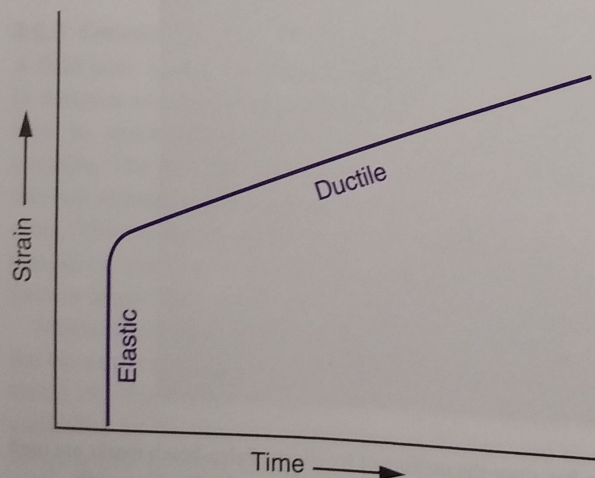
Figure 8.17 (a) Rate of rebound of Earth's lithosphere around Hudson Bay since the melting of ice sheets. Paleo-beach marks are used to measure rebound as a function of time. Using these data in Equation 8.34 yields a viscosity of ~10^{21} Pa·s for Earth's mantle. (b) Image of Ganymede (one of Jupiter's large moons). The yellow arrows indicate craters whose topography has relaxed. The rims, because they are smaller than the craters themselves, have not yet relaxed. The black arrows point to younger craters that have not relaxed, perhaps indicating a change in heat flow with time. NASA image.

linearly with stress as described by Young's modulus (E). We have treated ductile layers as fluids that also respond linearly to stress – deformation builds up with time, remains when the stress is removed, and the rate of deformation scales linearly with applied stress (i.e., Newtonian fluid) as described by dynamic viscosity (μ). Real geologic materials are more complex and often don't fit cleanly in one of these two categories.

8.7.1 Visco-Elastic Rheology

Rocks and ices near the surface of Earth or other planetary bodies are generally brittle – they respond elastically to stress until their strength is overcome, at which point they fracture. When rocks and ices are deep enough that the confining pressure is comparable to or greater than their strength, they can be ductile – they flow to achieve an equilibrium stress. In reality, rocks and ices in almost any situation exhibit a combination of these behaviors – a linear elastic response at first, followed by ductile flow, then fracturing if the stress overcomes the strength and confining pressure (see Figure 8.3). The dominant behavior we see in a specific situation often depends on the timescale involved.

Looking at this **visco-elastic** model as a function of time, we see that when a stress is first applied, elastic strain is incurred immediately. As that stress is maintained on the (nominally solid) object, strain continues to increase linearly with time as the object deforms ductilely (Figure 8.18). In other words, all solid geologic materials behave elastically over short timescales but, given sufficient time, will flow. A question that follows is: Over what timescales should we treat a given material as a solid versus as a fluid? A common way to answer this question is to find the time that it takes for the viscous (ductile) strain to equal the initial elastic strain. We can calculate this time by dividing the elastic strain by the viscous strain rate. Assuming linear elastic behavior as a solid and Newtonian (linear) behavior as a fluid, we find that this timescale is

$$\tau_M = \frac{\mu}{G_s} \tag{8.36}$$

where G_s is the shear modulus (or modulus of rigidity) as described in Section 8.2. This quantity is called the Maxwell time, after the same Maxwell who established the famous equations for electromagnetism. It seems that he was conducting long-term pendulum experiments, and those experiments were compromised by slow extension of the pendulum wire. The Maxwell time for the Earth's mantle is around 100 years, which explains why it transmits short period seismic waves like a solid, but is rebounding from the melting of ice sheets as a fluid. The Maxwell time of H_2O ice near its melting temperature is on the order of an hour; warm ice flows fairly readily under sustained stress.

8.7.2 Non-Newtonian Rheology

Some materials do not follow the linear Newtonian flow law defined in Equation 8.31, and the viscosity of almost all materials is temperature-dependent. The generalized relationship between stress and strain rate has the form

$$\dot{\varepsilon} = A\sigma^n d^{-m} e^{-\frac{E_a + PV_a}{RT}} \tag{8.37}$$

Here, d is grain size, E_a is an activation energy, V_a is an activation volume, A is a constant, R is the universal gas constant, and T is temperature. E_a, V_a, A, n, and m are determined from experiments. Compared to Equation 8.31, we can write an effective viscosity as

$$\mu_{\text{eff}} = \frac{\sigma}{\dot{\varepsilon}} = \frac{\sigma^{1-n} d^m}{A} e^{-\frac{E_a + PV_a}{RT}} \tag{8.38}$$

In this form, the viscosity of a material depends on the grain size of the material, the stress applied, the temperature, and several parameters intrinsic to the material.

Solid materials flow as reorganization occurs within the crystal lattice. This reorganization can happen in different ways, depending on the material, the stress applied, the temperature, etc. At relatively low stress, diffusion of defects or vacancies through the volume of the grains or along grain boundaries enables flows to occur. Both of these diffusion pathways tend to lead to Newtonian behavior ($n = 0$), but with different grain size dependences ($m = 2$ and 3, respectively). At higher pressures, dislocations within the crystal lattice migrate, leading to non-Newtonian behavior and different grain size dependencies.

Figure 8.18 Illustration of visco-elastic behavior. When a constant stress is applied and maintained, elastic strain occurs immediately, and viscous or ductile strain accrues linearly with time.

The temperature, stress, and grain size dependencies of flow behavior can make it difficult to apply insights gained from terrestrial geology to other planetary bodies. Jupiter's large moon Europa is a prime example. Planetary geologists would like to know whether convection in Europa's ice shell contributes to the complex geology on the surface. In fact, it has been suggested that plate tectonics may even occur on Europa, if it can be driven by convection in the ice shell (Kattenhorn and Prockter, 2014). Unfortunately, the effective viscosity of ice under the conditions at Europa are not well constrained. Even if the flow law itself were known, there is no way with current measurements to know the grain size in the ice shell. The effective viscosity is uncertain by orders of magnitude just from the uncertainty in grain size alone. Nevertheless, models do favor convection in Europa's ice shell, and these models will be tested in the next decade by NASA's *Europa Clipper* mission.

Summary

Geologic materials under stress strive for balance – they want to relieve that stress as effectively as they can. The way to relieve stress is through strain, and the strain that a material will undergo when stress is applied depends on its rheology. We have seen how planetary surfaces support topography and respond to surface loads. Detailed measurements of a body's gravity field provide a window into the interior, at least in terms of how mass is arranged below the surface. The observation from gravity measurements that the giant Tharsis volcanoes on Mars are not in isostatic balance indicates that the lithosphere must have been extremely thick and strong when they formed, and remains so now. Yet, relaxation of even relatively small craters on some regions of Saturn's small moon Enceladus reveals high internal heat flow in those regions in the past.

Planetary surfaces are solid and brittle, and heat transfer through them is by conduction. Surface temperatures are controlled primarily through solar heating and therefore change systematically over the course of a day and an orbit. Measurements of temperature as a function of time, which can be done remotely by measuring thermal flux emitted from the surface, provide a powerful means to determine properties of the surface, such as grain size and induration. Planetary interiors, however, often behave, at least over geologic timescales, as a fluid. Understanding fluid mechanics is therefore critical for assessing the dynamics of planetary interiors. One consequence of more fluid-like behavior is that heat may be transferred by convection. When convection occurs, it induces stress in the overlying lithosphere, the effects of which may be measurable by planetary geologists.

Review Questions

1. What does it mean to say that something is a linear elastic material? How are stress and strain related for a linear elastic material? How does strain in one dimension affect strain in another dimension?

2. Imagine a sedimentary basin on some planetary body that is confined on all sides and filled to a depth of 1 km. The horizontal strains, ε_{xx} and ε_{yy}, are both zero, and the vertical stress at any depth z in the basin is given by $\sigma_{zz} = \rho z g$. Use the constitutive relations in Equation 8.4 to find expressions for the strain in the vertical direction (ε_{zz}) and the stresses in the horizontal directions (σ_{xx} and σ_{yy}). Compute these quantities at depths of 0.1, 0.5, and 1.0 km for a sedimentary basin on Earth, assuming $\rho = 2100 \, \text{kg/m}^3$, $E = 50 \, \text{GPa}$, and $\nu = 0.2$. Now compute the same quantities for an icy sedimentary basin on Titan, where $g = 1.3 \, \text{m/s}^2$, $\rho = 917 \, \text{kg/m}^3$, $E = 10 \, \text{GPa}$, and $\nu = 0.3$. Compare the results for the two bodies.

3. The South Pole-Aitken (SPA) impact basin, located on the far side of the Moon, is about 8 km deep and appears to be in isostatic balance. Describe how you would use the principle of isostasy to compute the thickness of the crust surrounding the basin, under the assumption that the basin-forming impact excavated all the way to the mantle. For crustal and mantle densities of 2800 kg/m³ and 3400 kg/m³, respectively, compute the crustal thickness and discuss the reliability of this estimate.

4. Describe how to estimate the thickness of the lithosphere from topography near a big surface load. Use this technique to compute the elastic thickness (h) of the lithosphere on Europa from the data in Figure 8.8, assuming the plate is broken beneath the load, $g = 1.32$ m/s^2, $E = 10$ GPa, $\nu = 0.3$, $\rho_m = 1000$ kg/m^3, and there is no fill in the flexural basin ($\rho_{fill} = 0$). Compare your results to values of elastic thickness given in Figure 8.13 for the Pacific plate beneath the Hawaiian islands and the Ulfrun region of Venus.

5. How can topography and gravity measurements be combined to determine the compensation state of surface features?

6. Describe diurnal temperature variations at the surface and near-surface (top few meters) of planetary bodies.

7. Why are some craters on Ganymede, Enceladus, and other icy bodies not topographic lows? Why do they still have raised rims?

8. What does it mean to say that something is a Newtonian fluid? What are the various factors that affect the effective viscosity of geologic materials? Which of these factors imposes the largest uncertainty in estimating the viscosities of the mantles of other planets (i.e., besides Earth)? Compare and contrast the relative importance of each in the mantles of planetary bodies.

SUGGESTIONS FOR FURTHER READING

Gerya, T. (2010) *Introduction to Numerical Geodynamic Modelling.* Cambridge: Cambridge University Press. An excellent resource for delving more deeply into the computational techniques necessary for modern geophysics/geodynamics.

Stacey, F. D., and Davis, P. M. (2008) *Physics of the Earth.* Cambridge: Cambridge University Press. This book presents a complete history of the Earth from a geophysical perspective.

Turcotte, D., and Schubert, G. (2014) *Geodynamics*, 3rd edition. Cambridge: Cambridge University Press. The classic textbook for learning geodynamics for terrestrial and planetary applications. The third edition includes chapters and examples for computational modeling of geodynamical processes.

REFERENCES

Barnett, D. N., Nimmo, F., and McKenzie, D. (2002). Flexure of Venusian lithosphere measured from residual topography and gravity. *Journal of Geophysical Research* 107(E2). DOI: 10.1029/2000JE001398.

Bland, M. T., Singer, K. N., McKinnon, W. B., et al. (2012) Enceladus' extreme heat flux as revealed by its relaxed craters. *Geophysical Research Letters*, **39**, L17204.

Delbó, M., Libourel, G., Wilderson, J., et al. (2014) Thermal fatigue as the origin of regolith on small asteroids. *Nature*, **508**, 233–236.

Delbó, M., Mueller, M., Emery, J. P., et al. (2015) Asteroid thermophysical modeling. In *Asteroids IV*, eds. Michel, P., DeMeo, F., and Bottke, W. F. Tucson, AZ: University of Arizona Press, pp. 107–128.

Goutorbe, B., Poort, J., Lucazeau, F., et al. (2011) Global heat flow trends resolved from multiple geological and geophysical proxies. *Geophysical Journal International*, **187**, 1405–1419.

Hammond, N. P., Phillips, C. B., Nimmo, F., and Kattenhorn, S. A. (2013) Flexure on Dione: investigating subsurface structure and thermal history. *Icarus* **223**, 418–422.

Huppert, K. L., Royden, L. H., and Perron, J. T. (2015) Dominant influence of volcanic loading on vertical motions in the Hawaiian islands. *Earth and Planetary Science Letters*, **418**, 149–171.

Hurford, T. A., Beyer, R. A., Schmidt, B., et al. (2005) Flexure of Europa's lithosphere due to ridge loading. *Icarus*, **177**, 380–396.

Kattenhorn, S. A., and Prockter, L. M. (2014) Evidence for subduction in the ice shell of Europa. *Nature Geoscience*, **7**, 762–767.

Lemoine, F. G., Goossens, S., Sabaka, T., et al. (2014) GRGM900C: a degree 900 lunar gravity model from GRAIL primary and extended mission data. *Geophysical Research Letters*, **41**, 3382–3389.

McGovern, P. J., Solomon, S. C., Smith, D. E., et al. (2002) Localized gravity/topography admittance and correlation spectra on Mars: implications for regional and global evolution. *Journal of Geophysical Research*, **107**, E12.

Nimmo, F., and McKenzie, D. (1998) Volcanism and tectonics on Venus. *Annual Reviews of Earth and Planetary Science*, **26**, 23–51.

Turcotte, D., and Schubert, G. (2014) Geodynamics, 3rd edition. Cambridge: Cambridge University Press.

Watters, T. R. (2003) Lithospheric flexure and the origin of the dichotomy boundary on Mars. *Geology*, **31**, 271–275.

Zuber, M. T., Smith, D., Watkins, M., et al. (2013) Gravity field of the moon from the Gravity Recovery and Interior Laboratory (GRAIL) mission. *Science*, **339**, 668–671.